Research of the fluoridozirconate Na$_7$Zr$_6$F$_{31}$ structure and its crystal hydrates from the vibrational spectroscopy data

© E.I. Voit, N.A. Didenko

Institute of Chemistry, Far East Branch, Russian Academy of Sciences,
Vladivostok, Russia

e-mail: evoit@ich.dvo.ru

The structure and thermal stability of compounds in the Na$_7$Zr$_6$F$_{31}$ · nH$_2$O ($n = 0$, 6, 12) series were studied using infrared spectroscopy (IR), Raman scattering (Raman), differential thermal, thermogravimetric (DTA-TGA) and X-ray diffraction (XRD). The vibrational (IR, Raman) spectroscopy data for the compound Na$_7$Zr$_6$F$_{31}$ and its hydrates were obtained, systematized and summarized. The bands in the vibrational spectra of Na$_7$Zr$_6$F$_{31}$ were assigned based on quantum-chemical calculations. Taking into account the spectroscopic data, possible structural changes were proposed during mutual transitions Na$_7$Zr$_6$F$_{31}$ ↔Na$_7$Zr$_6$F$_{31}$ · nH$_2$O during hydration-dehydration.

Keywords: complex zirconium fluorides, sodium fluoridozirconates, thermogravimetry, vibrational spectroscopy.

Introduction

Phase formation in the ZrF$_4$ system with NaF is of interest for fabrication of multicomponent fluorozirconate glass that are used in fiber optics due to a wide transparency range [1]. In addition, the mixture of ZrF$_4$ and NaF is used as a fuel composition in nuclear reactors as stable to irradiation and having low melting temperature [2]. Some aspects of corrosion resistance of alloys in the ZrF$_4$–NaF melt are discussed in [3].

When sodium fluoride interacts with zirconium fluoride, some chemical compounds are formed: Na$_3$ZrF$_7$, Na$_5$Zr$_2$F$_{13}$, Na$_2$ZrF$_6$, Na$_3$Zr$_2$F$_{11}$, Na$_7$Zr$_6$F$_{31}$, Na$_3$Zr$_4$F$_{19}$ [4]. The ZrF$_4$-NaF system contains also three eutectics, two of which are low-melting, containing 40.5 mol.% and 49.5 mol.% ZrF$_4$ and melting at 505 and 512°C, respectively. In both cases, one of the salt mixture components is the phase Na$_7$Zr$_6$F$_{31}$.

Though F/Zr = 5.167 in sodium fluoridozirconate Na$_7$Zr$_6$F$_{31}$, it may be referred complex zirconium fluorides with F/Zr = 5. Crystalline structure of Na$_7$Zr$_6$F$_{31}$ (6NaZrF$_5$·NaF) is the three-dimensional frame [Zr$_6$F$_{30}$]$_n^{6n-}$ with additional ions Na$^+$ and F$^-$ (one for each cell) [5].

Formation of such compounds is typical not only for Zr, but also for all tetravalent equivalents of Zr — hafnium, thorium, uranium, neptunium, plutonium, etc. [6]. The family with the general formula M$_7^I$M$_6^{IV}$F$_{31}$ (M^I = Ag$^+$, Na$^+$, K$^+$, Tl$^+$, Rb$^+$, NH$_4^+$; M^{IV} = Zr^{4+}, Hf^{4+}, Ce^{4+}, Tb^{4+}, Pa^{4+}, U^{4+}, Np^{4+}, Th^{4+}) with the structural type Na$_7$Zr$_6$F$_{31}$ contains more that thirty known compounds, about a half of which are derivatives with cation Na$^+$. Note that the ionic radius ratio plays the key role in formation and stability of M$_7^I$M$_6^{IV}$F$_{31}$ compounds with different M^I and M^{IV} combinations [7].

M$_7$Zr$_6$F$_{31}$ fluoridozirconates are formed with Na$^+$ and K$^+$. Na(K)$_7$Zr$_6$F$_{31}$ crystallizes from the Na(K)F-ZrF$_4$ melt containing 46.2 mol.% ZrF$_4$ [4,8]. Na$_7$Zr$_6$F$_{31}$ melts congruently at 525°C. K$_7$Zr$_6$F$_{31}$ exists only in solid state below 380°C and above this temperature disintegrates to a mixture of KZrF$_5$ and K$_2$ZrF$_6$. It means that the thermal stability of M$_7$Zr$_6$F$_{31}$ (M = Na$^+$, K$^+$) decreases as the radius of the outer-sphere monovalent cation increases.

Investigation of phase formation in ZrO$_2$−H$_2$SO$_4$−NaF(HF)−H$_2$O [9] and ZrO(NO$_3$)$_2$−H$_3$PO$_4$−NaF(HF)−H$_2$O [10] water solutions has shown that in particular conditions one of the crystallizable phases is Na$_7$Zr$_6$F$_{31}$ · 12H$_2$O crystal hydrate (or the mixture of Na$_7$Zr$_6$F$_{31}$ and Na$_7$Zr$_6$F$_{31}$ · 12H$_2$O). Polyhydrate with the above-mentioned composition is currently a single example of a water-abundant fluoridozirconate crystal hydrate with a singly charged outer-sphere cation. This is attributed to a considerably smaller ionic radius and higher hydration energy of Na$^+$ [11,12]. With relatively high cation hydration enthalpy, the H$_2$O molecules compensate the cation's coordination capacity.

Among the sodium fluoridozirconates, Na$_7$Zr$_6$F$_{31}$ · 12H$_2$O is underexplored. Currently known infrared (IR) spectroscopy data for Na$_7$Zr$_6$F$_{31}$ · 12H$_2$O and the thermogram description [9] don't provide a full picture of its structure, thermal behavior and stages of Na$_7$Zr$_6$F$_{31}$ · 12H$_2$O transition to the anhydrous phase Na$_7$Zr$_6$F$_{31}$.

For the purpose of clarification, addition, systematization and generalization of data on the structure and thermal transformations of Na$_7$Zr$_6$F$_{31}$ · 12H$_2$O and products of partial (Na$_7$Zr$_6$F$_{31}$ · 6H$_2$O) and full (Na$_7$Zr$_6$F$_{31}$) dehydration, they have been investigated in this study using the infrared
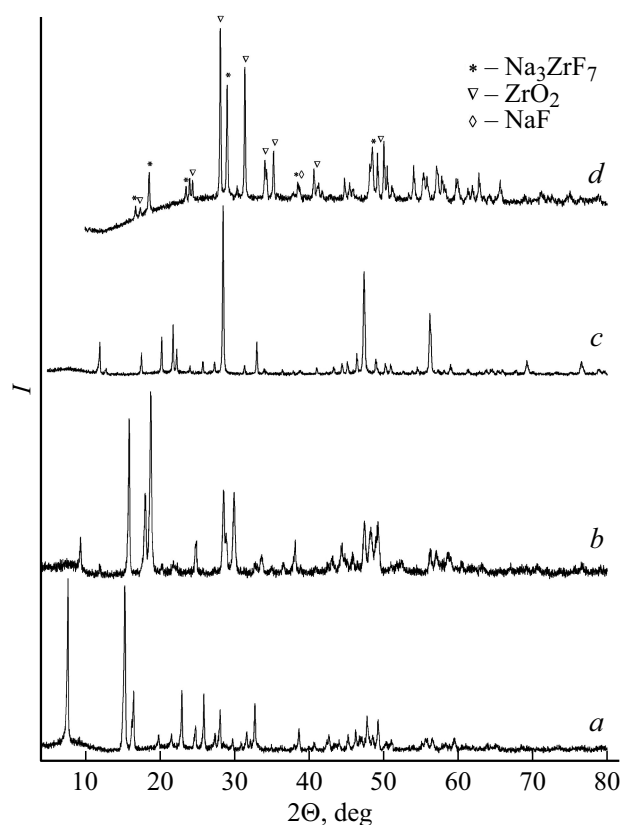
Figure 1. X-ray images of $Na_7Zr_6F_{31} \cdot 12H_2O$ (*a*) and its heating products up to 120 (*b*), 210 (*c*) and 500°C (*d*).

(IR) spectroscopy, Raman scattering (RS) and thermal analysis methods.

Experiment

Synthesis $Na_7Zr_6F_{31} \cdot 12H_2O$

5.34 g of zirconyl nitrate dihydrate (AR ≥ 99%) (0.02 mol) was solved in the mixture of 10 ml H_2O and 3 ml 40%-HF (ACS 99.99%) at room temperature. Sodium fluoride water solution was added portionwise to the prepared solution: 0.84 g (0.02 mol) to 15 ml H_2O previously acidified with some drops of 40%-HF to prevent hydrolysis of NaF (NaF/Zr = 1 : 1). Loose deposit forms immediately when the components are mixed and occupies the whole volume of the stock solution. The obtained deposit was filtered using the Buchner funnel, washed on the filter with a small amount of ice water, water with alcohol and dried at room temperature until air dried (at relative humidity ≈ 20%). Single-phase condition of the compound was supported by the X-ray diffraction analysis (XRD) method. The X-ray image of the obtained compound coincides with the X-ray image provided in [9] and corresponds to the hydrated $Na_7Zr_6F_{31} \cdot 12H_2O$ phase (Figure 1, *a*). Diffraction pattern of $Na_7Zr_6F_{31} \cdot 12H_2O$ is not available in PDF-2 database.

Thermal analysis of the prepared compound was carried out using the Q-1000 MOM derivatograph in air at a heating rate of 5 deg/min. The weighed amount of the sample was 110 mg. Ignited Al_2O_3 was used as a reference standard.

$Na_7Zr_6F_{31} \cdot 6H_2O$ and $Na_7Zr_6F_{31}$ were obtained by thermal dehydration of dodecahydrate during heating in the derivatograph at a rate of 2.5 deg/min up to 120 and 215°C, respectively.

X-ray diffraction data for the compounds was obtained using the „STOESTADIP" (CuK$_{\alpha1}$-radiation, $\lambda = 1.5406$, germanium monochromator) and BrukerD8 ADVANCE (CuK$_{\alpha}$-radiation, graphite monochromator) diffractometers. PDF-2 powder data bank was used to obtain the product composition information.

Infrared spectra were obtained at $4000-400\,cm^{-1}$ at room temperature using the IR-Affinity instrument on KRS-5 window for samples prepared as a paraffin oil suspension. RS spectra of the examined compounds were recorded using the WiTec alpha500 Raman microscope (laser wavelength $\lambda = 532\,nm$).

To assign the bands in $Na_7Zr_6F_{31} \cdot nH_2O$ spectra, quantum-chemical calculations were performed using GAMESS software package [13] . The calculations were performed within the local density functional theory combined with the B3lyp exchange-correlation potential. The LANL2dz basis set with core potential for Zr(IV) and Na atoms and the 631g* basis function set for F atoms were used. Model clusters were chosen taking into account the known structural data. The equilibrium geometry and normal vibration frequencies were calculated in the harmonic approximation. The results were obtained using the equipment of the Center „Far-Eastern Computing Resource" at the Institute of Automation and Control Processes, Far-East Branch of the Russian Academy of sciences (https://cc.dvo.ru).

Results and discussion

Differential thermal and thermogravimetric analysis

Dehydration of water-abundant salt hydrates is known to take place at high water vapor pressure with salt solution melting and boiling off, at medium pressure — step-by-step, but with other intermediate hydrates and without melting [14]. Dehydration of $Na_7Zr_6F_{31} \cdot 12H_2O$ also goes in a different way when the heating conditions are changed.

By heating slowly $Na_7Zr_6F_{31} \cdot 12H_2O$ at a rate of 2.5 deg/min, the solid-phase dehydration is performed in two stages (Figure 2). The first stage goes in the range of 48−114°C with the maximum rate at 82°C and 7.3% loss of weight, which corresponds to removal of 6 H_2O molecules per formula unit ($\Delta m_{calc} = 7.14\%$). Thus, partial dehydration of the water-abundant crystal hydrate by heating at a relatively low rate up to 114−115°C leads to formation of an intermediate hydrated $Na_7Zr_6F_{31} \cdot 6H_2O$ phase that has an individual X-ray pattern (Figure 1).
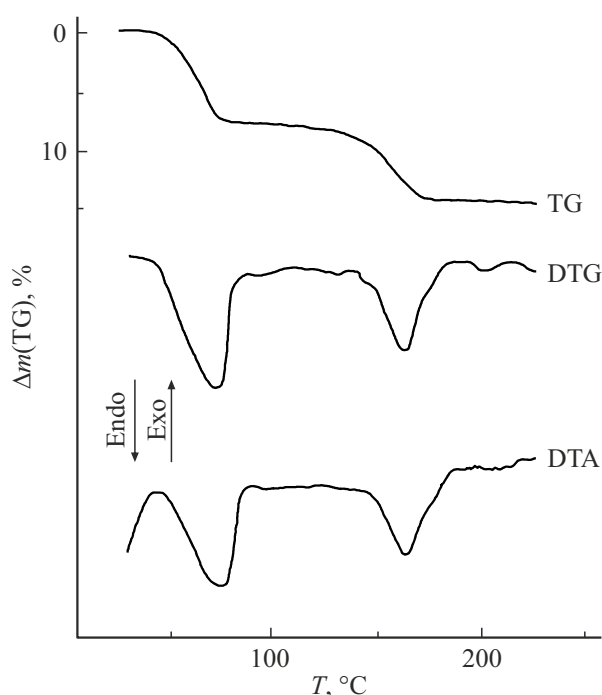
Figure 2. Thermal curves of $Na_7Zr_6F_{31} \cdot 12H_2O$.

The second dehydration stage goes in the range of $120-215°C$ with the maximum rate at $154°C$ and 14.2% total loss of weight, which corresponds to removal of 12 H_2O molecules per formula unit ($\Delta m_{calc} = 14.29\%$). As a result of this thermal treatment of $Na_7Zr_6F_{31} \cdot 12H_2O$, loose anhydrous $Na_7Zr_6F_{31}$ is obtained (card № 00-022-1417(C)) according to XRD (Figure 1).

In case of non-equilibrium dehydration conditions (fast heating, variation of P_{H_2O}, hindered diffusion), when the heating rate increases up to 5 deg/min, the dehydration behavior of $Na_7Zr_6F_{31} \cdot 12H_2O$ varies. dehydration flows in one stage in the range of $50-200°C$ with the maximum rate at $90°C$. An overcooling wave at $80-85°C$ is recorded on the T-curve. This is due to he fact that the dehydration process occurs only when the crystal hydrate decomposes into salt and water with the saturated salt solution boiled off. When heating up to $200°C$, the loss of weight is 13.1%. After heating, the sample is non-loose, viscous within the sample, and air-drying, which is proved by formation of a liquid phase during dehydration in this case. $Na_7Zr_6F_{31}$ phase is also the obtained product according to the XRD data.

Further heating of $Na_7Zr_6F_{31}$ in the range of $220-480°C$ leads to gradual loss of weight due to removal of residual water and start of pyrohydrolysis of the anhydrous compound by air moisture. The total loss of weight during heating up to $460-480°C$ is $16-17\%$. The incorporation of oxygen into the lattice of the compound is possible in the form of isomorphic impurity with partial substitution of fluorine and/or the formation of particles of an independent oxide phase ZrO_2. According to the XRD data, the heating

product contains the impurity phase ZrO_2 (monoclinic) together with $Na_7Zr_6F_{31}$.

Increase in the pyrohydrolysis degree of $Na_7Zr_6F_{31}$ is observed during isothermal curing of $Na_7Zr_6F_{31} \cdot 12H_2O$ at $500°C$ (boundary temperature before the start of melting of the anhydrous compound) in air in a muffle furnace during three hours to the oven-dry weight. The total loss of weight in this case is 26.0%. According to the XRD data, as a result of the above-mentioned thermal treatment, $Na_7Zr_6F_{31}$ is fully transformed to a mixture o phases — tetragonal Na_3ZrF_7 (card 01-074-0808(C)) and monoclinic ZrO_2 (card 00-013-0307(D)) with a higher content of the latter (Figure 1).

In this case, the hydrolytic decomposition of anhydrous $Na_7Zr_6F_{31}$ is described by the general reaction:

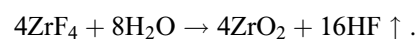$$Na_7Zr_6F_{31} + 8H_2O \rightarrow 2Na_3ZrF_7 + 4ZrO_2 + NaF + 16HF \uparrow .$$
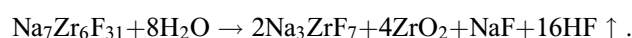
The total estimated loss of weight is 25.96%. The most intensive reflection of the NaF(cub.) phase with $d = 2.32\,Å$ overlaps with one of the reflections of Na_3ZrF_7.

Probably, during isothermal heating of $Na_7Zr_6F_{31}$ in air ($T = 500°C$), weakening of the cation-anion interactions and growing of dynamic processes in both sublattices results in gradual thermal dissociation of the compound and disproportionation to fluorine and cation, which may be represented by the following reactions:

$$Na_7Zr_6F_{31}(6NaZrF_5 \cdot NaF) \rightarrow 6NaZrF_5 + NaF,$$

$$6NaZrF_5 \rightarrow 2Na_3ZrF_7 + 4ZrF_4.$$
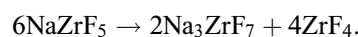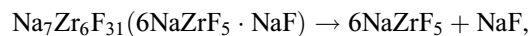
The resultant ZrF_4 is subjected to pyrohydrolysis.

$$4ZrF_4 + 8H_2O \rightarrow 4ZrO_2 + 16HF \uparrow .$$

Thus, at the first stage, the expected thermal decomposition scheme of $Na_7Zr_6F_{31}$ in air is described by the general overall equation:

$$Na_7Zr_6F_{31} + 8H_2O \rightarrow 2Na_3ZrF_7 + 4ZrO_2 + NaF + 16HF \uparrow .$$

Then as a result of further heating, the resulting intermediate fluoride phase Na_3ZrF_7 decomposes interacting with water vapor from air:

$$Na_3ZrF_7 + 2H_2O \rightarrow ZrO_2 + 3NaF + 4HF \uparrow .$$

According to the X-ray diffraction pattern, the product of further heating of $Na_7Zr_6F_{31} \cdot 12H_2O$ up to $800°C$ in air is preferably a mixture of ZrO_2 and NaF with a small content of Na_3ZrF_7. The loss of weight is 30.7%. In case of complete hydrolytic decomposition of $Na_7Zr_6F_{31} \cdot 12H_2O$ into ZrO_2 and NaF, the estimated volatile yield is 31.75%.

X-ray structural analysis data

Prior to the analysis of $Na_7Zr_6F_{31} \cdot 12H_2O$ crystal hydrate with unknown structure, it is reasonable to examine the
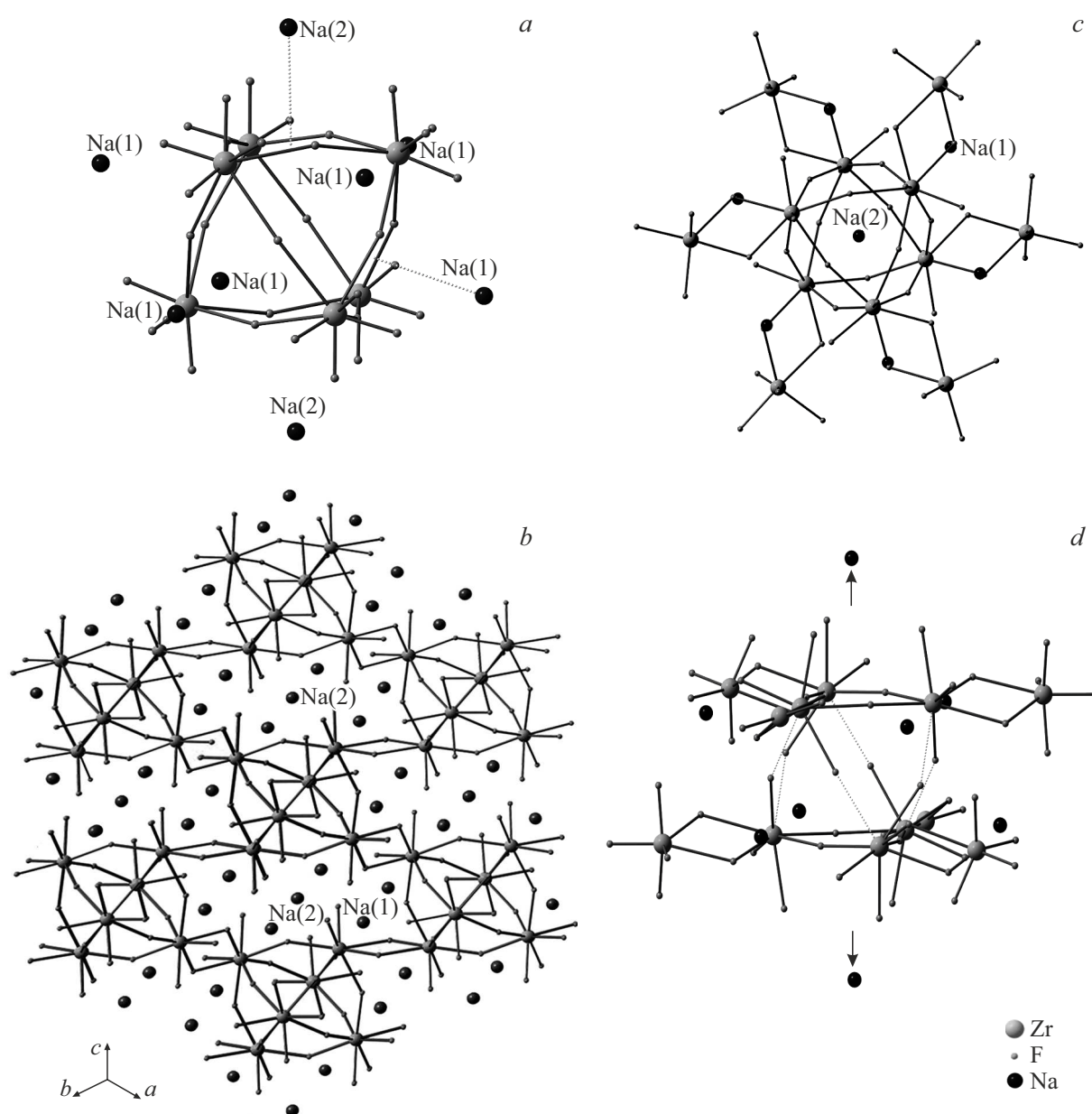
Figure 3. Cuboctahedral grouping of Na$_8$Zr$_6$F$_{36}^{4-}$ in cation environment (*a*). Fragment of Na$_7$Zr$_6$F$_{31}$ structure (*b*). Model grouping of Na$_8$Zr$_{12}$F$_{60}^{4-}$ (S_6) (*c*). Separation of the model grouping when Na(2) cations are moved(*d*).

structure of anhydrous Na$_7$Zr$_6$F$_{31}$ first because it is the predecessor of the water-abundant hydrated phase.

Na$_7$Zr$_6$F$_{31}$ (Na$_6$Zr$_6$F$_{30}$·NaF) (CN of Zr = 8) crystallizes in space group $R\bar{3}$ ($Z = 3$) with lattice parameters: $a = 13.807$ Å, $c = 9.429$ Å. Zr-F bond lengths vary from 2.031 to 2.179 Å [5]. Anion of Na$_7$Zr$_6$F$_{31}$ has a framework structure. Each six Zr polyhedra joined by common F-bridged apexes (ZrF$_m$ (Δ)) forms a typical cuboctahedral grouping (ZrF$_8$)$_6$ (Figure 3, *a*). This grouping is connected to six identical groupings through the external edges of the Zr polyhedra leading to formation of the three-dimensional [Zr$_6$F$_{30}$]$_n^{6n-}$ frame. Additional F$^-$ ion is placed in a cuboctahedral void (distance Zr-F(6) = 2.63Å) and is positionally

disordered [5]. Na(2)$^+$ cations are placed in the center of the hexagonal channel and surrounded octahedrally by six end F atoms (Na-F distance is 2.461 Å) from two neighboring (ZrF$_8$)$_6$ groupings on the *c* axis. Interatomic distances between Na(2)...Na(2) in the Na$_7$Zr$_6$F$_{31}$ structure are equal to 9.429 Å. Na(1)$^+$ cations (six per cell) are evenly distributed in the *ab* plane and surround the (ZrF$_8$)$_6$ groupings, they coordinate seven fluorine atoms (distances vary from Na−F to 2.342−2.516 Å).

The Na$_7$Zr$_6$F$_{31}$ structure may be also written as a three-dimensional network consisting of separate layers in the *ab* plane that contain three-membered metal rings combined into 12-membered Zr polyherda rings [15]. Next separated
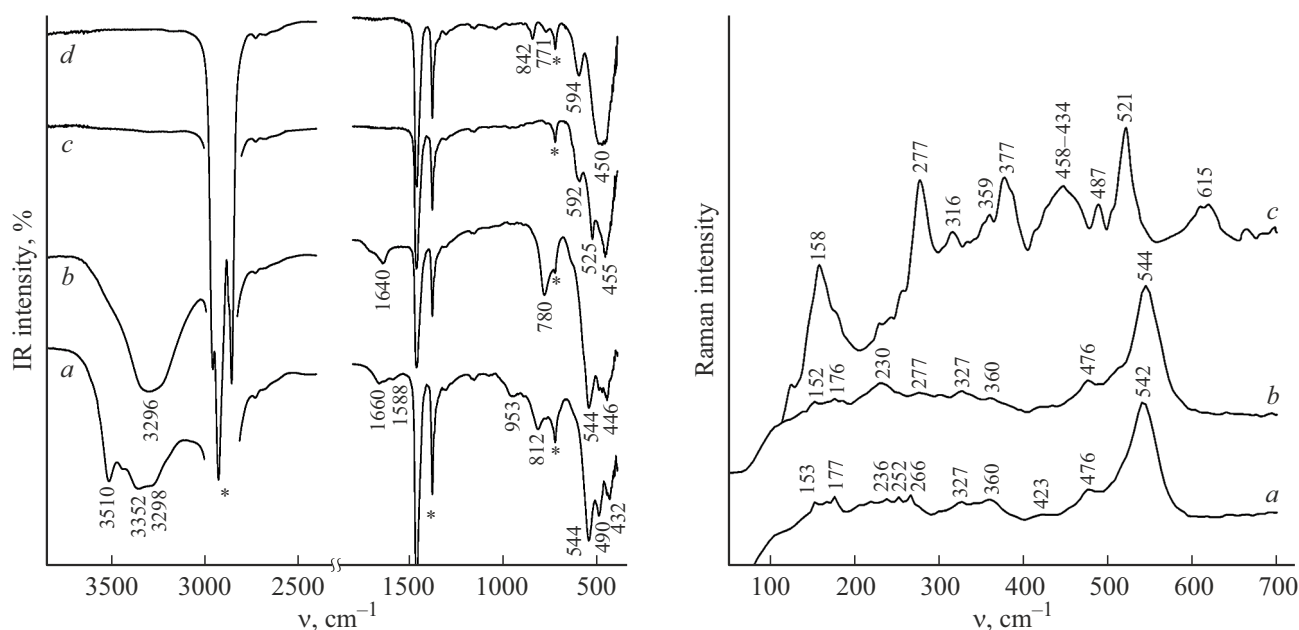
Figure 4. Infrared spectra and RS spectra of $Na_7Zr_6F_{31} \cdot 12H_2O$ (*a*), $Na_7Zr_6F_{31} \cdot 6H_2O$ (*b*), $Na_7Zr_6F_{31}$ (*c*), heating product up to $460°C$ (*d*). Asterisks on curve *a* (IR spectrum) show the absorption bands of the paraffin oil.

layers are bound through the apexes with formation of bilayers composed of cubooctahedra staggered along the *c* axis (Figure 3, *b*). Stepped arrangement of the layers creates hexagonal channels where Na^+ cations are placed. As far as interlayer bonds in some layers are rather strong, and interlayer forces are relatively weak, some layers are expected to serve as a single whole during exchange or hydration reactions, and interlayer distances may easily vary.

Vibrational spectroscopy

$Na_7Zr_6F_{31}$

Structure of the discussed anhydrous compound was examined using the vibrational (IR, RS) spectroscopy methods together with quantum chemical calculations (Figure 4, 5). In the isolated state, the $[Zr_6F_{36}]^{12-}$ cubooctahedron has the symmetry T_h (Figure 3, *a*). Its vibrational spectrum, including translational and rotational modes (symmetries T_u and T_g, respectively) are described by the irreducible representation $\Gamma_{Th} = 6A_g + 4A_u + 6E_g + 4E_u + 15T_g + 17T_u$.

In the $Na_7Zr_6F_{31}$ structure, cubooctahedra are interconnected by bridged edge bonds ($ZrF_m(P)$) and surrounded by cations, which reduces their local symmetry in ideal case to S_6. Six $Na(1)$ cations are arranged between the edge bonds and two $Na(2)$ cations interact with end F_k atoms. Thus, each cubooctahedron has eight triangular faces with Na^+ cations opposite them. According to the structural data for $Na_7Zr_6F_{31}$, the $Na_8Zr_{12}F_{60}^{4-}$ model cluster, in which cation-anion environment is considered (Figure 3, *c*), was chosen for calculation. In the equilibrium geometry of the $Na_8Zr_{12}F_{60}^{4-}$ (S_6) model cluster, two distances to the
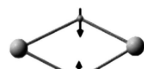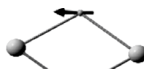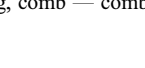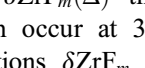
common F_m-apex in the Zr-F_m-Zr fragment are different. In triangular faces lying opposite to $Na(2)$, the Zr-Zr distances are equal to 4.278 Å, the Zr-F_m-Zr distances are equal to 2.139, 2.200 Å, the Zr-F_k distances are equal to- 1.987, 1.997 Å. For faces opposite $Na(1)$: the Zr-Zr distances are equal to 4.297 Å, the Zr-F_m-Zr distances are equal to 2.24, 2.22 Å, and the common edge — Zr-F_m — 2.194, 2.221 Å.

In the equilibrium geometry of the $Na_8Zr_{12}F_{60}^{4-}$ cluster, positions of six external Zr groupings in the $Na_8Zr_{12}F_{60}^{4-}$ cluster were frozen and vibration frequencies of the $[Zr_6F_{36}]^{12-}$ (S_6) grouping were calculated. When the local symmetry of the cubooctahedral $[Zr_6F_{36}]^{12-}$ grouping ($T_h \rightarrow S_6$) decreases, the triply-degenerate vibrational modes are split: $T_g \rightarrow A_g + E_g$ and $T_u \rightarrow A_u + E_u$. For a simplified representation, frequencies are grouped by the prevailing contributions to the corresponding vibration (Table). As can be seen, the cluster effect occurs, i.e. in each band there are similar frequen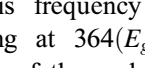cies, including possible symmetric and asymmetric combinations of characteristic vibrations of the Zr polyhedra and various structural members.

In the calculated IR spectrum of the cubooctahedral $[Zr_6F_{36}]^{12-}$ grouping, three groups of active bands of stretching vibrations with the symmetry A_u, E_u: $\nu_s ZrF_8$ (611, 588 cm^{-1}), $\nu_{as} ZrF_k$ (532, 529 cm^{-1}), induced mainly by the end bond vibrations, and νZrF_m (482, 472 cm^{-1}) with the main contribution of the bridge bond vibrations in triangular faces.

According to the calculations, $\nu_s ZrF_8$, $\nu_{as} ZrF_k$ modes are the most intense in the RS spectrum, the corresponding frequencies are ~ 608, 600 (A_g, E_g) and 528, 524

Experimental position of bans (cm^{-1}) in spectra of $Na_7Zr_6F_{31}$, calculated vibration frequencies (cm^{-1}) of the $[Zr_6F_{36}]^{12-}$ grouping in the $Na_8Zr_{12}F_{60}^{4-}$ cluster and their assignment

Experiment* $Na_7Zr_6F_{31}$		Calculation $Na_8Zr_{12}F_{60}^{4-}$, (S_6)			Assignment**	
IR, ν	RS, ν	ν	Symmetry	Intensity		
592 cp		611, 588	E_u, A_u	5.0, 6.7	comb $\nu_s ZrF_8$	
	615 wd m	608, 600	A_g, E_g	41.0, 24.0		
525 c		532, 529	A_u, E_u	17.3, 16.5	comb $\nu(ZrF_7$-$F_k)$ or $\nu_{as} ZrF_k$	
	521 c	528, 524	A_g, E_g	26.2, 2.5	$\nu_{as} ZrF_k$	
		482, 472	E_u, A_u	9.3, 7.7	$\nu ZrF_m (\Delta) + \nu F_k$	
	487 w	485	E_g	9.2		
455 oc		444, 446	E_u, A_u	0.7, 1.0	$\delta_{sc} ZrF_m (P)$ ν_s F-F	
	458 wd m	447, 444	A_g, E_g	10.8, 17.2		
	428 w	395, 361	E_u, A_u	21.7, 2.8	$\nu ZrF_m(\Delta)+\nu ZrF_m(P)$	
		424, 402	A_g, E_g	19.3, 4.2		
		388, 356	A_u, E_u	1.4, 0.6	$\nu ZrF_m(\Delta) + \nu ZrF_m(P)$	
	380 arm	396, 375	A_g, E_g	3.7, 22.1		
		393, 332	A_u, A_u	0.1, 0.1	$\delta ZrF_m(\Delta)$	
		329, 324	E_u, E_u	1.1, 3.3		
	377 m	378, 348, 333	A_g, A_g, E_g	26.3, 13.8, 1.6		
		368, 365	A_u, E_u	0.5, 1.3	$\nu_{as} ZrF_m (P)+\nu ZrF_m(\Delta)$	
	359 w	364, 360	E_g, A_g	16.2, 3.4		
		312, 306, 305	A_u, A_u, E_u	0.1, 2.8, 4.0	ωZrF_k, $\delta_{sc} F_k$	
	316 w	336, 320	A_g, A_g	13.3, 6.7		
		318, 307	E_g, E_g	18.2, 14.0		
		292, 289	A_u E_u	0.0, 4.6	ρZrF_m, $\omega ZrF_m(P)$	
		269, 264	A_u, E_u	2.8, 0.1		
		304, 294	A_g, $E_g A_g$	41.0, 31.8		
	277 s	278, 267	A_g, E_g	22.0, 15.0		
		246, 228	A_g E_g	49.0, 26.0	twZrF_m (P) +twZrF_k	
		228, 206	A_g, E_g	17.0 40.0		
		247, 225	A_u, E_u	2.2, 1.0		
		229, 227	E_u, A_u	0.0, 0.0		
		202	E_u	0.7	ρZrF_k	
		214, 202	E_g, A_g	32.0, 3.3		
		192, 191	E_u, A_u	0.3, 0.0	ρZrF_8	
		187, 175	E_g, A_g	14.0, 0.0		
			$5A_u$, $5E_u$		ν, δZrF_8	
	158 s wd	178 and lower	$5A_u$, $5E_g$	–		

* Symbols used for the recorded bands: o — very strong, s — strong, m —moderate intensity, w — weak, arm — arm, wd — wide.

** Symbols used for vibrations: ν — stretching, δ — deformation, δ_{sc} — scissoring, ω — wagging, tw — torsional, ρ — rocking, comb — combinations.

(A_g, E_g) cm^{-1} (Table, Figure 5). The calculated frequencies of the stretching vibrations $\nu ZrF_m(\Delta)$ and deformation vibrations $\delta ZrF_m(\Delta)$ at $490-470$ and $400-330$ cm^{-1}, respectively, may be considered as a typical sign of the presence of triangular faces in the $Na_7Zr_6F_{31}$ structure.

Symmetric deformation vibrations $\delta ZrF_m(\Delta)$ that are the most intense in the RS spectrum occur at $378(A_g)$ and $375(E_g)$ cm^{-1}. Stretching vibrations δZrF_m (P) of the edge bonds also fall within this frequency range with the most intense of them lying at $364(E_g)$ and $360(A_g)$ cm^{-1}. Deformation vibrations of the end $Zr-F_k$
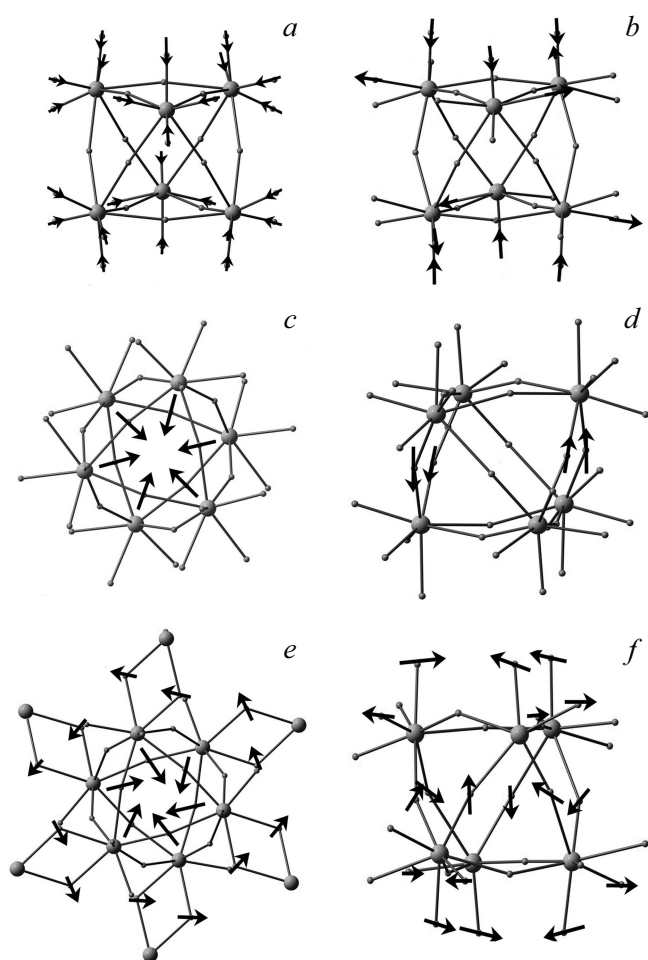
Figure 5. Combinations of $[Zr_6F_{36}]^{12-}$ vibrations active in the RS spectrum with peaks at 608 (*a*), 528 (*b*), 378 (*c*), 375 (*d*), 304 (*e*), 246 (*f*) cm^{-1}.

and edge Zr$-$2F$_m$$-$Zr bonds are below in frequency, with breathing modes $\sim$ 304 (A_g) and 246 (A_g) cm^{-1} being the most intense of them (Figure 5, *e,f*). These vibrations cause forced vibrations of bridge bonds in the triangular faces. Among the lattice modes, the most intense one is the breathing (A_g) mode ν(ZrF$_8$)$_6$ associated with the simultaneous translational motion of each of the ZrF$_8$ groupings towards each other, and occurs at 160 cm^{-1} according to the calculation data.

The experimental IR spectrum of Na$_7$Zr$_6$F$_{31}$ contains no vibration bands of the H$_2$O molecules (Figure 4, curve *c*). Characteristic modes of complex fluoridozirconate anions are below 700 cm^{-1} [16]. In accordance with the calculated data, the band with the peak at 525 cm^{-1} is assigned to the stretching vibrations ν_{as}ZrF$_k$ of the end bonds, and the wide intense band with the peak at 455 cm^{-1} is probably a composite one and is assigned to the stretching vibrations of bridge bonds in the triangular faces νZrF$_m$(Δ) and to the vibrations of bridge bonds in the edge δ_sZrF$_m$(P).

The peak at $\sim$ 521 cm^{-1} in the experimental RS spectrum is attributed to the prevailing contribution of the

breathing mode combination ν_{as}ZrF$_k$(A_g). The broadened band with the peak at 615 cm^{-1} is assigned to symmetric combinations ν_sZrF$_8$ of the Zr polyhedra in a cubooctahedron. The presence of bands $\sim$ 377 and 359 cm^{-1} in the spectrum (mainly group vibrations δZrF$_m$(Δ) and νZrF$_m$(Δ)) proves that there are cubooctahedra in the structure of the examined Na$_7$Zr$_6$F$_{31}$.

Note that similar vibrational spectra have oxofluoridozirconates M$_2$Zr$_3$OF$_{12}$ (M = Tl, Rb, K, NH$_4$), except the characteristic line ν_{as}ZrO at 670 cm^{-1} from the Zr$_3$O fragment [17]. M$_2$Zr$_3$OF$_{12}$ whose structure contains the hexanuclear Zr$_6$F$_{30}$O$_4$ grouping (CN of Zr = 8) [18,19] feature close structural proximity with the examined Na$_7$Zr$_6$F$_{31}$ (derivatives from the fluorite structure with the structural unit M$_6$F$_{32}$ [15,20]).

Comparing the structures of Na$_7$Zr$_6$F$_{31}$ and M$_2$Zr$_3$OF$_{12}$ (M = Tl$^+$, K$^+$, NH$_4^+$), it should be noted that in oxofluoridozirconates the oxigen atom in the metal ring (Zr$_3$O) stabilizes the layered anion sublattice. And in Na$_7$Zr$_6$F$_{31}$, additional bonding of the Z polyhedra in the metal rings (ZrF$_8$)$_6$ is performed by the excess fluorine ion placed in the cuboctahedral void. In view of this, one can assume that, when Na$_7$Zr$_6$F$_{31}$ is heated in air as a result of pyrohydrolysis, at the initial stage (T = 460°C) partial isomorphic substitution of the excess F$^-$ ion with the oxygen ion takes place with generation of additional Zr-O-Zr bonds, while the initial framework structure in the oxofluoride phase [Na$_6$Zr$_6$F$_{30}$·Na(O,F)] is maintained. In the IR spectrum of the heating product (460°C), bands occur at 842 and 771 cm^{-1} (Figure 4, curve *d*). These bands are assigned to the vibrations of Zr$-$O, respectively, in the oxofluoride and oxide phases of ZrO$_2$.

Na$_7$Zr$_6$F$_{31}$ · 12H$_2$O

Full hydration of Na$_7$Zr$_6$F$_{31}$ with transition to the highest crystal hydrate Na$_7$Zr$_6$F$_{31}$ · 12H$_2$O is followed by the attachment of crystallization water molecules that presumably in a different way surround the non-equivalent Na(1) and Na(2) cations in the initial salt structure.

The X-ray image of Na$_7$Zr$_6$F$_{31}$ · 12H$_2$O differs distinctively (Figure 1) from the X-ray image of the anhydrous compound. Position of the first intense diffraction reflection at the angles 2Θ = 7.74° characterizes the value of the basal interplanar spacing d_{001} = 11.43 Å in the hydrated phase. The presence of reflections that are multiple of it with indices d_{002} = 5.57 Å and d_{003} = 3.86 Å is indicative of a typically layered structure of the hydrated phase. For layered compounds, d_{001} coincides with parameter*c* of the lattice cell and directly correlates with the interlayer distance.

To clarify the nature of structural variations in the transition Na$_7$Zr$_6$F$_{31}$ →Na$_7$Zr$_6$F$_{31}$·12H$_2$O, the Na$_8$Zr$_{12}$F$_{60}^{4-}$(S_6) model grouping was calculated, where two Na(2) atoms are put away from each other, according to the X-ray image, at a distance of 11.43 Å and their positions are frozen (Figure 3, *d*). In the optimized geometry of the Na$_8$Zr$_{12}$F$_{60}^{4-}$ cluster, two triangular faces opposite the Na(2)

atoms are slightly compressed (distances Zr...Zr 4.220 Å, Zr-F$_m$ 2.114, 2.147 Å). Bridge bonds in the triangular side faces of a cubooctahedron (opposite the Na(1) atoms) — increase greatly (distances Zr...Zr 4.428 Å, Zr-F$_m$ 2.206, 2.387 Å). In the limiting case, the bridge bonds of the side faces are broken and individual anion fragments containing three-membered metal rings $(ZrF_7)_3$ are formed. In this case the coordination number (CN) of Zr decreases to 7, and the number of end F$_k$ atoms in each Zr polyhedra increases.

In the experimental IR spectrum of Na₇Zr₆F₃₁ · 12H₂O (Figure 4, curve *a*) in the area of stretching vibrations of the H₂O molecules (νOH) , there are two pairs of bands with peaks at 3510, 3431 and 3352, 3298 cm^{-1} that are identified as relatively weak and more strong H-bonds [21, 22]. Two sets of bands are also present at 1588, 1660 and 953, 812 cm^{-1} and are assigned to deformation vibrations δHOH and librational vibrations of the H₂O molecules, respectively. The presence of two sets of bands in the spectrum may be explained by the presence of two types of crystallization water molecules included in the coordination environment of the non-equivalent Na(1) and Na(2) cations in the polyhydrate structure.

One can assume that in transition Na₇Zr₆F₃₁ →Na₇Zr₆F₃₁ · 12H₂O, contacts Na(2)-F are broken and the Na(2) cations are coordinated by six H₂O molecules with formation of hydrated $[Na(2)(H_2O)_6]^+$ cations. When the Na₇Zr₆F₃₁ →Na₇Zr₆F₃₁ · 12H₂O structure transforms into a layered structure, the number of interlayer contacts Na(1)-F decreases and it becomes possible to attach one H₂O molecule to each Na(1) cation. When there is a short contact Na-OH₂, Na(1)$^+$ cations may exert polarizing influence on the water molecule leading to formation of strong H-bonds O-H...F, which is proved by the IR spectra. Thus, in the experimental IR spectrum, the set of bands 3510−3431, 1588 and 812 cm^{-1} may be assigned to the vibrations of the H₂O molecules of the $[Na(2)(H_2O)_6]^+$ grouping. And the second group of bands with the peaks at 3352−3298, 1660 and 953 cm^{-1} is assigned to the vibrations of the H₂O molecules coordinating the Na(1)$^+$ cations.

In the spectra of Na₇Zr₆F₃₁ · 12H₂O in the area of anion vibrations, half-width and intensity of the bands with peaks ∼ 544 (IR) and ∼ 542 (RS) cm^{-1} increase (Figure 4, curve *a*), which is probably associated with the proximity of the mode combinations ν_sZrF₇ and ν_{as}ZrF$_k$ in frequency and is attributed to the presence of cyclic trimeric fragments.

In transition to the crystal hydrate, the shift of 521 → 544 cm^{-1} lines is indicative of strengthening of Zr-F$_k$ bonds in the Zr polyhedra. The presence of bands νZrF$_m(\Delta)$ ∼ 490 cm^{-1} (IR) and 476 cm^{-1} (RS) is associated with the presence of cyclic trimeric fragments both in the anhydrous compound structure and in the crystal hydrate structure (Table). Broadening and diffusivity of the RS bands in the area of deformation vibrations (290−200 cm^{-1}) with the involvement of the end bonds

Zr−F$_k$ may be explained by a ramified system of O-H...F type H-bonds in the hydrate structure.

Thus, Na₇Zr₆F₃₁ · 12H₂O has presumably a layered structure. Anion layers containing three-membered metal rings are alternated with interlayers of hydrated Na$^+$ cations. Non-equivalent Na(1) and Na(2) cations are bound in aquacomplexes with different hydrate numbers. The Na(1) atom has a mixed hydrate-fluoride environment, and the Na(2) has a hydrate environment. The excess F$^-$ ion is likely positioned in the interlayer space and is involved in the O-H...F type H-bonds.

Na₇Zr₆F₃₁ · 6H₂O

Dehydration mechanism in the transition Na₇Zr₆F₃₁ · 12H₂O→Na₇Zr₆F₃₁ · 6H₂O may be described by the motion of the Na(2) ions that are free from their H₂O ligands to a position that enables cations to bind with the end F atoms of the anion complex. Thus, in the Na₇Zr₆F₃₁ · 6H₂O structure, the Na(2) cations change their hydrate environment to fluoride one with CN equal to 6. Moreover, the Na(1) cation interlayer with the mixed hydrate-fluoride environment probably prevents from incorporation of the Zr polyhedra into cubooctahedra.

In the X-ray diffraction pattern of Na₇Zr₆F₃₁·6H₂O, the first diffraction peak shifts to 9.37 Å, which may be explained by the proximity of anion layers in the lattice of the partially dehydrated phase (Figure 1).

With partial dehydration of Na₇Zr₆F₃₁ · 12H₂O→Na₇Zr₆F₃₁ · 6H₂O, the IR spectrum of the latter is simplified in the area of vibrations of the H₂O molecules (Figure 4, curve *b*). νOH bands of weakly bound H₂O molecules disappear in the Na(2) coordination. There are only the vibration bands of the H₂O molecules that coordinate the Na(1)$^+$ cations. There is a symmetric wide intense band with a peak at 3296 cm^{-1} that corresponds to stretching of the same-type H₂O molecules involved in strong O-H...F type H-bonds. The presence of one water libration band at 780 cm^{-1} also proves that strong H-bonds are formed. The deformation vibration δHOH is shown as a wide band at 1640 cm^{-1} with a high-frequency arm. The H₂O molecules in the salt structure are probably exposed to strong disturbing effect of the Na$^+$ ions [22].

IR and RS spectra of Na₇Zr₆F₃₁ · 12H₂O and Na₇Zr₆F₃₁ · 6H₂O in the anion vibration area are very similar, which emphasizes the closeness of their anion sublattice structures.

Conclusions

Dehydration and thermal stability processes in Na₇Zr₆F₃₁ · 12H₂O have been investigated in a wide temperature range. It has been found that water in the water-abundant crystal hydrate is separated into two types by the temperature of water removal from the structure. As a result of partial and full dehydration when heated

to 115 and 215°C, respectively, the intermediate hydrated $Na_7Zr_6F_{31} \cdot 6H_2O$ phase and anhydrous $Na_7Zr_6F_{31}$ are formed.

The vibrational spectroscopy methods have been used to study the influence of the hydrate number of the outer-sphere cation on the anion sublattice structure of the $Na_7Zr_6F_{31} \cdot nH_2O$ crystal hydrates ($n = 12, 6$). It is shown that a similar layered structure of anion sublattices with CN of Zr equal to 7 is implemented in crystal hydrates. During full dehydration and transition to anhydrous $Na_7Zr_6F_{31}$, the structure is transformed into a frame one with CN of Zr increasing to 8. According to the quantum-chemical calculations, assignment of the bands in the vibrational spectra of $Na_7Zr_6F_{31}$ has been performed.

Funding

Conflict of interest

The authors declare that they have no conflict of interest.

References

[1] J.-L. Adam. J. Fluor. Chem., **107**, 265 (2001). DOI: 10.1016/S0022-1139(00)00368-7

[2] G.N. Yakovlev, E.F. Myasoedov, L.D. Dukhovenskaya, V.I. Silin. Radiokhimiya **21**, (5), 687 (1979) (in Russian).

[3] V.M. Azhazha, A.A. Andriiko, A.S. Bakai, S.V. Volkov, S.V. Devyatkin, A.N. Dovbnya, S.D. Lavrinenko, A.A. Omelchuk, B.M. Shirokov. Voprosy atomnoy nauki i tekhniki. Seriya: Fizika radiatsionnykh povrezhdenij i radiatsionnoe materialovedenie **86**, (3), 134 (2005). (in Russian)

[4] C.J. Barton, W.R. Grimes, H. Insley, R.E. Moore, R.E. Thoma. J. Phys. Chem., **62**, 665 (1958). DOI: 10.1021/j150564a008

[5] J.H. Burns, R.D. Ellison, H.A. Levy. Acta Cryst., B**24** (2), 230 (1968). DOI: 10.1107/S0567740868002013

[6] E.M. Moulakou. *Synthéses, caractérisations structurales et physico-chimiques de fluoruresd' eléments tétravalents* (Université Blaise Pascal, Clermont-Ferrand, 2007). 167 p.

[7] Ch.C. Underwood, C.D. McMillen, J.W. Kolis. J. Chem. Crystallogr., **44**, 493 (2014). DOI: 10.1007/s10870-014-0532-4

[8] A.V. Novoselova, Yu.M. Korenev, Yu.P. Simonov. DAN SSSR, **139** (4), 892 (1961). (in Russian)

[9] M.M. Godneva, D.L. Motov, V.Ya. Kuznetsov, N.L. Mikhailova. Zhurn. neorg. khimii, **47** (1), 119 (2002) (in Russian).

[10] M.M. Godneva, V.Ya. Kuznetsov, M.P. Rys'kina, V.V. Semushin, N.L. Mikhailova. Zhurn. neorg. khimii, **59**(8), 1071 (2014) (in Russian).

[11] R.D. Shannon. Acta Cryst., A**32**, 751 (1976). DOI: 10.1107/S0567739476001551

[12] Y. Marcus. J. Chem. Soc. Faraday Trans., **87**(18), 2995 (1991). DOI: 10.1039/ft9918702995

[13] M.W. Schmidt, K.K. Baldridge, J.A. Boatz, S.T. Elbert, M.S. Gordon, J.H. Jensen, S. Koseki, N. Matsunaga, K.A. Nguyen, S. Su, T.L. Windus, M. Dupuis, J.A. Montgomery. // J. Comput. Chem., **14**, 1347 (1993). DOI: 10.1002/jcc.540141112

[14] V.A. Logvinenko, F. Paulik, I. Paulik *Kvaziravnovesnaya termogravimetriya v sovremennoi neorganicheskoi khimii* (Nauka, Novosibirsk, 1989) (in Russian).

[15] M. Leblanc, V. Maisonneuve, A. Tressaud. Chem. Rev., **115** (2), 1191 (2015). DOI: 10.1021/cr500173c

[16] E.I. Voit, N.A. Didenko, K.N Galkin. Opt. and spectr., **118** (1), 97 (2015). DOI: 10.7868/S0030403415010262

[17] E.I. Voit, N.A. Didenko, K.A. Gayvoronskaya. Opt. and spectr., **124**(3), 333 (2018). DOI: 10.61011/0000000000

[18] I. Mansouri, D. Avignant. J. Solid State Chem., **51**, 91 (1984). DOI: 10.1016/0022-4596(84)90319-014.

[19] M.A. Saada, A. Hemon-Ribaud, V. Maisonneuve, L.S. Smiri, M. Leblanc. Acta Cryst., E**59**, 131 (2003). DOI: 10.1107/S1600536803018567

[20] E.A. Zhurova, B.A. Maximov, V.I. Simonov, B.P. Sobolev. Kristallografiya, **41**, 433 (1996). DOI: 10.1134/1.170440

[21] T. Seki, K.Y. Chiang, C.X. Yu, M. Okuno, J. Hunger, Y. Nagata, M. Bonn. J. Phys. Chem. Lett., **11**, (19), 8459 (2020). DOI: 10.1021/acs.jpclett.0c01259

[22] O.V. Sizova, V.I. Baranovsky. Zhurn. strukturn. khimii, **29**(1), 168 (1988).

Translated by E.Ilinskaya